Chapter 16
Research on Portable Methane Telemetry System Based on TDLAS

Jianguo Jiang, Junkai Hu, and Chunlei Jiang

Abstract This work studies the key technology of a non-contact and long-distance methane-measuring instrument based on tunable diode laser absorption spectroscopy (TDLAS) due to the difficulties in real-time monitoring of methane leaks over a large area and the challenges of installing sensors. Using Beer–Lambert law as the theoretical basis, the spectral line information of methane gas recorded in the high-resolution transmission (HITRAN) database is compared to select the mature light source technology of the 1653.72 nm absorption line. Through simulation and analysis of the optical path within the detection distance of 0–100 m, the size of the optical system is designed to be minimized, and the sensor can be installed in portable equipment or monitoring probes. A reference gas chamber is specially designed in the optical components to provide a feedback optical signal for the system to eliminate the fluctuation of the light source signal and achieve automatic peak searching. The detection accuracy within ten meters is improved from 200 to 130 ppm, and the dynamic monitoring accuracy is maintained at 0.3–3.6% with a detection speed of one second. After multiple experiments, the system is proven to be stable and reliable with fast response speed, which meets the requirements of real-time methane gas detection applications.

16.1 Introduction

Methane has a wide range of applications, but when the concentration reaches a certain level and mixes with oxygen, it can cause explosions, fires, and other safety accidents, seriously endangering life and property safety [1]. In order to avoid huge losses of personnel and property during production and prevent serious atmospheric pollution caused by methane gas leaks [2, 3], monitoring methane distribution and leakage is of great significance in preventing accidents and leaks.

J. Jiang · J. Hu (✉) · C. Jiang
Northeast Petroleum University, Daqing Heilongjiang 163318, China
e-mail: hujunkai_nepu@163.com

R. Kountchev et al. (eds.), *Proceedings of International Conference on Artificial Intelligence and Communication Technologies (ICAICT 2023)*, Smart Innovation, Systems and Technologies 368, https://doi.org/10.1007/978-981-99-6641-7_16

Traditional detection methods [4–7] have serious drawbacks in terms of inability to remote sensing and a large number of blind spots in regional monitoring inspections. Compared with traditional detection methods, tunable diode laser absorption spectroscopy (TDLAS) technology has the advantages of high sensitivity, fast response, and detection of large space measurements [8–10]. Based on the TDLAS technology with an open-cavity detection method, this paper builds a detection system that can achieve remote sensing and improves the open optical path design. The added auxiliary gas chamber and reflector are used to achieve automatic peak searching through feedback signals, effectively improving the system's response speed and measurement accuracy.

16.2 Working Principle of Telemetry System

16.2.1 Beer–Lambert Law

When a specific light source is irradiated onto methane gas, the vibration of the molecules in the ground state of the methane gas changes, which is essentially caused by the change in dipole moment of the molecule due to the photon energy. Radiant frequencies of the light cause strong absorption of energy by the gas molecules and lead to transition, resulting in a strong absorption peak at a specific frequency on the spectrum of the light source. This shows the relationship between the strength of the absorption of a substance to a certain wavelength of light and the concentration of the absorbing substance and the thickness of its gas layer. When the laser beam passes through the gas layer, the difference between the outgoing and incoming light intensity is directly proportional to the amount of gas molecules, and the concentration of the gas can be calculated by determining the variation in the intensity of the incoming and outgoing light. This relationship is described by Beer–Lambert law as shown in the equation.

$$\mathrm{I}_t(\lambda) = \mathrm{I}_0(\lambda)\exp(-\alpha(\lambda)\mathrm{LC}) \tag{16.1}$$

where I_t is the output light intensity, I_0 is the input light intensity, C represents the concentration of the gas to be measured, L represents the optical path length. $\alpha(\lambda)$ represents the gas absorption coefficient, and it is expressed as:

$$a(\lambda) = S(T)\varphi(\lambda)N \tag{16.2}$$

$S(T)$ is the linear intensity of the gas absorption line; $\varphi(\lambda)$ is linear absorption function; N is the molecular density of the gas.

The linear intensity of the gas absorption spectral line can be obtained by querying the high-resolution transmission (HITRAN) molecular absorption database [11]. Common line shape functions include Lorentzian, Gaussian, and Voigt functions [12,

13]. Based on the characteristics of these three functions, when the remote sensing system works under normal temperature and pressure, the calculation results of the Lorentzian function tend to be closer to the Voigt function. In this state, the error of the function is small and the trend is good, so the Lorentzian line shape function is selected as the line shape absorption function for modeling and simulation. Converting the concentration according to Eq. (16.1) gives Eq. (16.3):

$$c = \frac{1}{a(\lambda)PL} \ln \frac{I_0}{I_t} \tag{16.3}$$

According to Eq. (16.3), the gas concentration is related to the absorption coefficient, pressure, optical path, and incident and transmitted light intensities. After the gas to be measured is determined, the absorption coefficient of the gas can be obtained by querying the HITRAN database [11]. Then, by digitally measuring the light intensity of the incident and transmitted light, the gas concentration within the optical path can be calculated. Using this theorem, selective measurement of methane gas mixed in the air can be achieved. The Beer–Lambert law provides the most basic theoretical support for gas concentration detection.

16.2.2 Selection of CH_4 Absorption Line

Selecting appropriate methane (CH_4) absorption lines can effectively improve the measurement accuracy of the methane leak telemetry system and reduce the impact of background interfering gases on the system detection accuracy. The selection of absorption lines mainly considers two aspects. First, interfering gases such as vapor (H_2O) and carbon dioxide (CO_2) in the air. Since nitrogen (N_2) and oxygen (O_2) have different elements from methane, the spectral absorption lines differ greatly, and nitrogen and oxygen can be excluded from the interference source. Second, the laser must meet the limitations of current technological processes, and the laser component costs are expensive. Selecting lasers with higher frequencies can reduce the cost of portable devices. Refer to the HITRAN 2022 database [11] to obtain all absorption lines in the visible and infrared wavelength range of 10–26,315 cm^{-1} as shown in Fig. 16.1, excluding all isotopes and locking the CH_4 absorption line at the peak point of the absorption line strength parameter of 6046.96 cm^{-1} (1653.7235 nm) and 1.455e-21 cm^{-1} mol^{-1} cm^{-2}.

16.3 Detection System Design

According to Beer–Lambert's law, methane gas can also selectively absorb specific frequencies of lasers. By using direct absorption spectroscopy (DAS), the absorption spectrum of the target gas molecule can be obtained, and concentration analysis

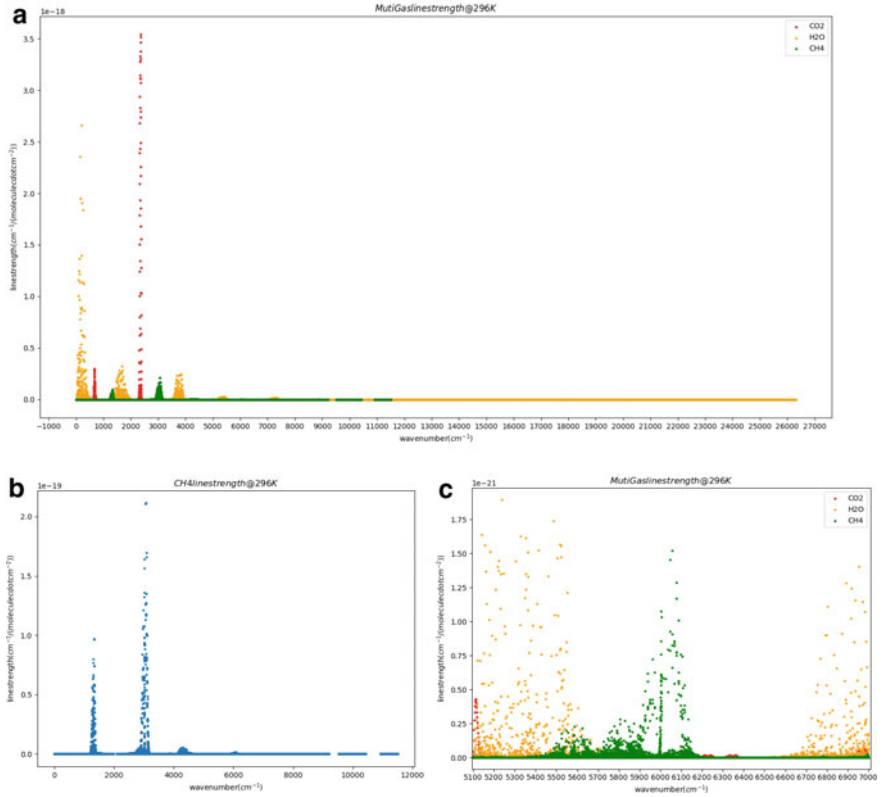

Fig. 16.1 Absorption lines of CH_4 in different ranges. **a** Absorption lines of H_2O, CO_2, and CH_4 in the range of 0–26,315 cm^{-1}; **b** absorption line of CH_4 in the range of 0–26,315 cm^{-1}; **c** absorption spectrum of CH_4 in the range of 5100–7000 cm^{-1}

can also be performed [14]. However, this method is only applicable in low-noise environments, and complex interference sources in open optical paths cannot be eliminated, so it cannot be effectively applied to remote sensing systems. The principle of wavelength modulation spectroscopy (WMS) technology was proposed by Reid and Labile [15], which extracts the second harmonics (2f) signal by a lock-in amplifier to filter out most of the interference noise. Compared with direct absorption spectroscopy, it more intuitively displays the relationship between gas concentration and signal peak, greatly reducing the noise of the detection system. The detection system design diagram is shown in Fig. 16.2, which consists of an optical part for methane detection and an electronic circuit for TDLAS signal processing. The function of low-pass Filter (LPF) is to obtain a higher signal-to-noise ratio (SNR) for the phase-locked amplifier.

Distributed feedback laser (DFB) is the most critical component in TDLAS technology, and the entire hardware system design is actually centered around the DFB laser. The methane absorption peak is very narrow, and there is no laser that can

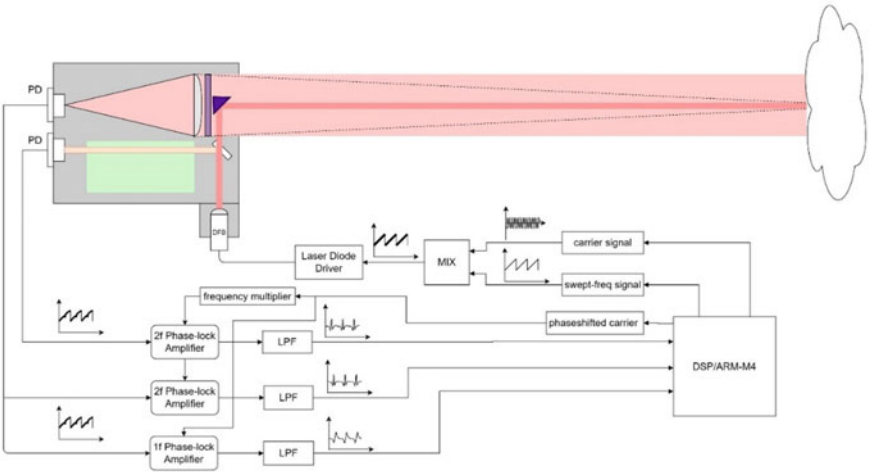

Fig. 16.2 Diagram of wavelength modulation technique for remote sensing system

continuously output precise 1653.7 nm laser. The DFB laser has the characteristic of wavelength controlled by the driving current. The embedded component generates a 38 kHz modulation carrier and a 5 Hz sweep signal, which is modulated by a mixer. The DFB emission current is controlled by the laser driver, with a driving current of 25–40 mA. The laser wavelength is adjusted by controlling the driving current of the DFB laser until it coincides with the absorption peak. As shown in Fig. 16.3, to ensure the stability of the light source, the DFB laser must be precisely temperature-controlled. The LPF in the figure plays the same role as in Fig. 16.2.

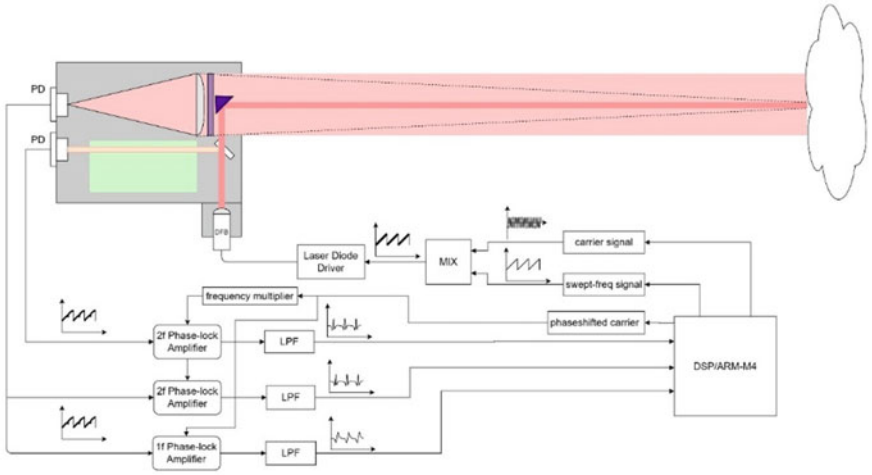

Fig. 16.3 Temperature–wavelength relationship curve

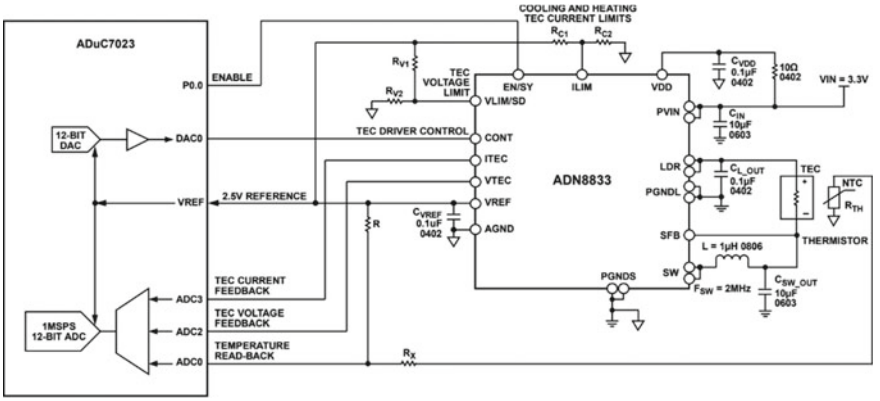

Fig. 16.4 Schematic diagram of ADN8833 drive circuit

After cost and control performance comparison, ADN8833 controller was ultimately chosen as the thermos-electric cooler (TEC) controller for the laser tube. ADN8833 reads the feedback voltage of the thermistor and provides a driving voltage to the TEC, with the microcontroller monitoring and controlling the thermal loop as shown in Fig. 16.4.

16.4 Optical System Design and Simulation

16.4.1 Optical Component Design

The infrared light emitted by the DFB is reflected by a total internal reflection right-angle reflector and directed toward a white diffuse reflection target. The diffuse light spot at the target forms a real image at 50.04–55 mm behind the collecting lens. The signal strength of the spot on the photodiode (PD) sensor mainly depends on the distance to the target and the scattering loss. The installation positions of the laser optical components are shown in Fig. 16.5, with the collimating lens made of K9L material and the filter using a 1653 nm narrowband filter.

16.4.2 Simulation and Verification of Optical Systems

When a high concentration of methane gas appears in the target area, the laser is emitted from the photosensitive window, passes through the measured space, and reaches the target. The light spot on the target is projected onto the PD1 through the collecting lens. The optical design of the telemetry system needs to consider

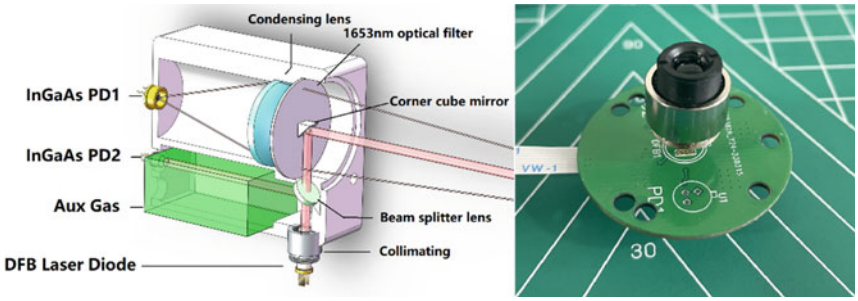

Fig. 16.5 3D design of the optical system and installed collimator DFB components

the position and size of the imaging spot on the photosensitive element surface of the lens for different placement positions of the reflecting target surface. To avoid uncontrollable factors beyond the design range during the actual adjustment of the components, ray-optics software is used to simulate the optical path and determine the optical path of the sensor photosensitive interface under each target position. Due to the limitation of the overall design size, the focal length of the lens is limited to 50 mm and the lens diameter is 50 mm, and the result is shown in Fig. 16.6.

The effective reception efficiency of the fiber at the receiving surface of the element is calculated according to the optical imaging calculation principle. Besides, based on the calculation of a 50 mm focal length and 50 mm diameter lens, the optimal measurement distance is 0.1–4 m, and the phototube can receive a maximum of 300 uA photocurrent, which is of great significance for the design of the photoelectric receiving circuit and the selection of the analog to digital converter (ADC) (Fig. 16.7).

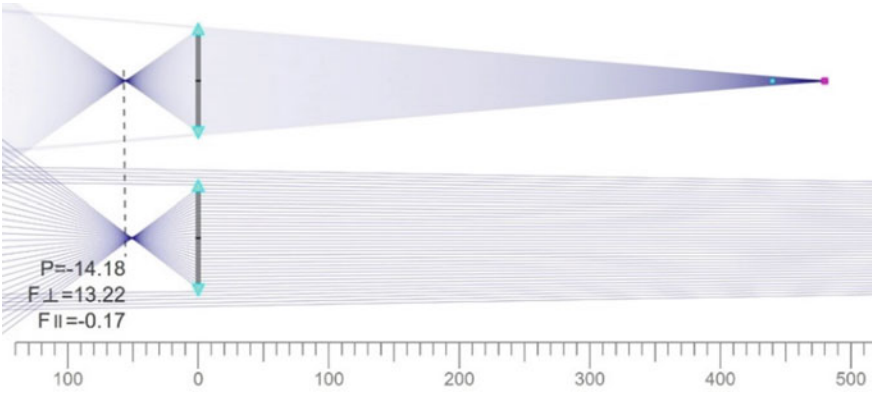

Fig. 16.6 Imaging optical path of the condenser at a distance of 0.5 and 50 m from the reflective surface

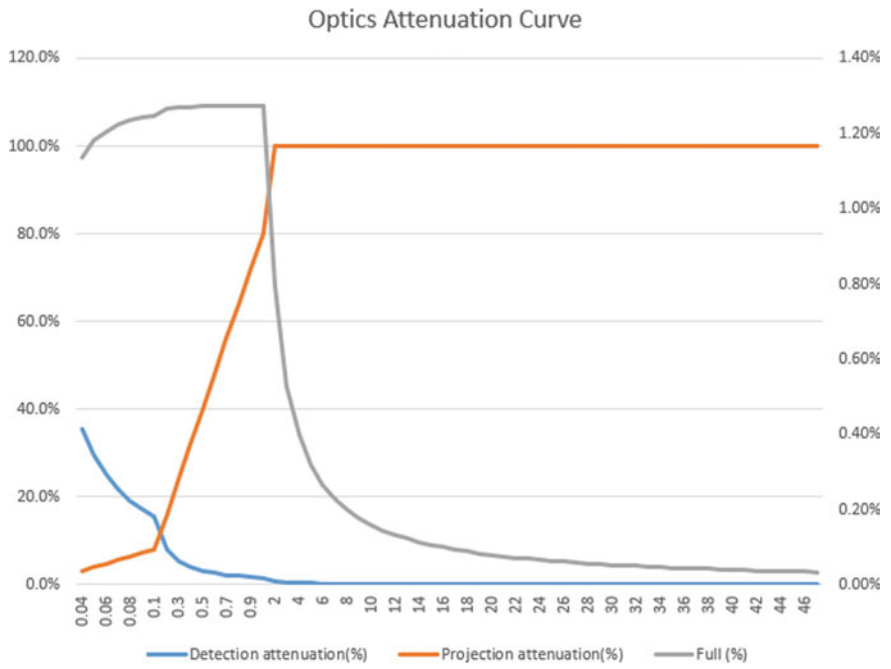

Fig. 16.7 Effect of imaging distance on the light intensity received by the sensor

16.5 Methane Concentration Detection Experiments

Experimental method: Using nitrogen as the balance gas, different concentration gas bags were obtained through a gas distribution device at 1 atm (1 atm = 101,325 Pa) to simulate methane plumes in actual detection scenarios. The arrangement of the gas plumes in the experiment is shown in Fig. 16.8.

Signal acquisition part is ultimately using NI PXle-6366 as the acquisition card for observing processed waveforms. The upper computer uses PCI-1DA 1.5.1 for analysis. The open-cavity remote sensing system differs from the inhalation detection device. The concentration calculation results will be expressed in ppm.m form. According to the Beer–Lambert law, the longer the optical path, the higher the absorption peak signal intensity. However, under diffuse reflection imaging, the farther the distance, the lower the received signal intensity, until it is difficult to distinguish. To verify the instrument stability, it is necessary to first calibrate the relationship between the voltage amplitude of the absorption spectrum line and the concentration, and then measure the same concentration gas bag at different distances and compare the data results.

Fig. 16.8 Gas bag simulating a leaked gas plume

16.5.1 Measurement Calibration

Nitrogen was used as the background gas for the measurement experiment. A gas distribution system was built using a precision flow meter, and five gas samples of different concentrations, namely 987, 1000, 1500, 5000, and 10,000 ppm, were prepared. The second harmonic signals of the extracted methane gas at different concentrations are shown in Fig. 16.9.

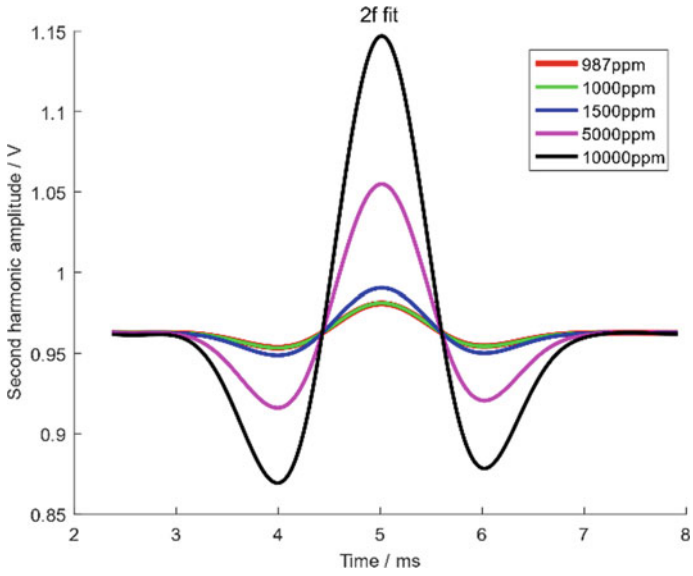

Fig. 16.9 2f signal intensity curves at different concentrations

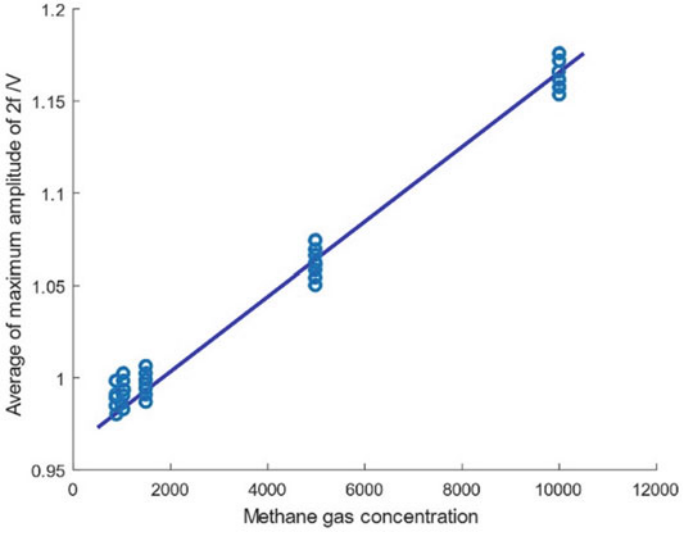

Fig. 16.10 Relationship between methane gas concentration and 2f signal intensity

Multiple measurements at different concentrations are required to obtain the median average value of ten sets of second harmonic signals for each concentration. There is a good linear relationship between the light intensity and the electrical signal generated by the sensor. By linear fitting, the data relationship between the median average value of the second harmonic amplitude (Amp) of the received light intensity signal and the methane gas concentration is obtained (see Fig. 16.10).

The fitting curve equation is Eq. (16.4):

$$C = 4484.0514 \cdot \max(\text{Amp}) - 0.9628 \tag{16.4}$$

According to the Beer–Lambert law, the absorption line strength is positively correlated with concentration. The 2f signal does not change the linear relationship between line strength and concentration. The calibration parameters obtained by linear fitting can be effectively used for the detection device.

16.5.2 Gas Measurement Accuracy Experiments

Standard concentrations of methane gas at 81.6, 90.9, 136.4, 454.5, and 909.1 ppm.m are prepared, and the signal concentrations are measured and calculated to determine the errors between the true and measured gas concentrations as given in Table 16.1. Based on observation, the relative errors between the true and measured gas concentrations are all within 7%. Furthermore, as shown in Fig. 16.11, the 2f harmonic amplitude still maintains a good linear relationship with the methane gas concentration.

Table 16.1 Relative error between proportioned concentration and measured concentration of standard methane gas

Item	Gas strength/ppm.m				
	81.6	90.9	136.4	454.5	909.1
Average 2f Amp/V	0.9805	0.9845	0.9953	1.0668	1.1634
Measuring concentration/ppm.m	79.1339	97.4669	145.7474	465.9606	899.0523
Relative error (%)	3.0	7.2	6.9	2.5	1.1

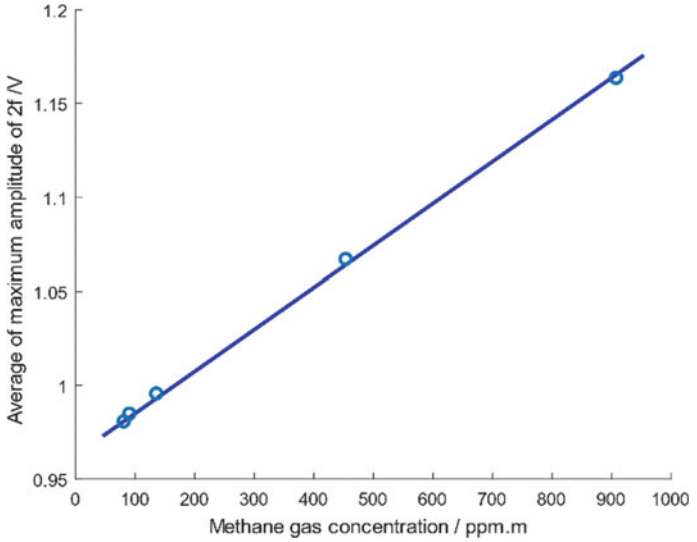

Fig. 16.11 Actual measurement concentration measurement linearity

According to the data in the table, the relative error between the real concentration of the measured gas and the concentration calculated by the measured signal is within 7.2%. It can be seen from the figure that the amplitude of the second harmonic and the concentration of methane gas still maintain a good linear relationship.

16.6 Summary

With TDLAS technology as the research background for remote measurement of methane gas concentration, wavelength modulation technology is used to suppress noise and improve detection accuracy. Furthermore, the mechanical structure of the sensor and the positioning of optical components are determined through simulation. Specifically, a precise flow meter was used in the experiment to mix samples for calibration, and through multiple experiments, a linear mathematical relationship

between the peak-to-peak value of the second harmonic signal and the methane gas concentration was determined. The experiment was repeated with other standard concentration gases to determine the actual error range of the detection system is less than 8%, which meets the requirements for industrial safety monitoring 16, proving the engineering application value of the device.

Acknowledgements This article was supported by grants from the Funding. Natural Science Foundation of Heilongjiang Province (LH2021F008).

References

1. Greenfield, P.F., Batstone, D.J.: Anaerobic digestion: impact of future GHG mitigation policies on methane generation and usage. Water Sci. Technol. J. Int. Assoc. Water Pollut. Res. **52**(1–2), 39–47 (2005)
2. Akimoto, H.: Global air quality and pollution. Science (2003)
3. Hodgkinson, J., Tatam, R.P.: Optical gas sensing: a review. Meas. Sci. Technol. **24**, 012004 (2013)
4. Dosi, M., Lau, I., Zhuang, Y., Simakov, D., Fowler, M.W., Pope, A.: Ultra-sensitive electrochemical methane sensors based on solid polymer electrolyte-infused laser-induced graphene. ACS Appl. Mater. Interfaces. **11**(6), 6166–6173 (2019)
5. Wan, H., Yin, H.Y., Lin, L., Zeng, X.Q., Mason, A.J.: Miniaturized planar room temperature ionic liquid electrochemical gas sensor for rapid multiple gas pollutants monitoring. Sens. Actuators, B Chem. **255**(1), 638–646 (2018)
6. Sha, M., Ma, X., Li, N., Luo, F., Fayer, M.D.: Dynamical properties of a room temperature ionic liquid: using molecular dynamics simulations to implement a dynamic ion cage model. J. Chem. Phys. **151**(15), 154502 (2019)
7. Zeng, X.: Ionic liquids: solvents and electrolytes for chemical sensor development. In: The 14th Beijing Conference and Exhibition on Instrumental Analysis (BCEIA 2011)
8. Shen, S., Li, W., Wang, M., Wang, D., Li, Y., Li, D.: Methane near-infrared laser remote detection under non-cooperative target condition based on harmonic waveform recognition. Infrared Phys. Technol. **120**, 103977 (2022)
9. Lu, J.Y., Hong, L., Dong, Y., Zhang, Y.S.: A new wavelet threshold function and denoising application. Math. Probl. Eng. **2016**(5), 1–8 (2016)
10. Benoy, T., Lengden, M., Stewart, G., Johnstone, W.: Recovery of absorption line shapes with correction for the wavelength modulation characteristics of DFB lasers. IEEE Photonics J. **8**(3), 1–17 (2016)
11. Mellau, G.C., Makhnev, V.Y., Gordon, I.E., Zobov, N.F., Tennyson, J., Polyansky, O.L.: An experimentally-accurate and complete room-temperature infrared HCN line-list for the HITRAN database. J. Quant. Spectrosc. Radiat. Transfer **279**, 107666 (2021)
12. Wahlquist, H.: Modulation broadening of unsaturated Lorentzian lines. J. Chem. Phys. **35**(5), 1708–1710 (1961)
13. Hu, C., X. Chen, Z. Li.: The gas temperature compensation research based on TDLAS technology. In: Chan, A.P.C., Hong, W.C., Mellal, M.A. (eds.) The 3rd International Conference on Material, Mechanical and Manufacturing Engineering 2015, AES, Atlantis Press, Netherlands (2015)
14. Reid, J., Labrie, D.: Second-harmonic detection with tunable diode lasers—comparison of experiment and theory. Appl. Phys. **26**, 203–210 (1981)
15. Standardization Administration of the People's Republic of China. GB/T 33672–2017 Cavity Ring-Down Spectroscopy system for measurement of atmospheric methane (2017)